IEEE Access
Multidisciplinary | Rapid Review | Open Access Journal

IEEE POWER & ENERGY SOCIETY SECTION

Received 13 September 2022, accepted 24 September 2022, date of publication 30 September 2022,
date of current version 11 October 2022.

Digital Object Identifier 10.1109/ACCESS.2022.3210949

RESEARCH ARTICLE

Effective Inertial Response With New Coordinated Control for Multiple WPPs

SUNGHOON LIM[1], (Member, IEEE), DONGHEE CHOI[2], (Member, IEEE), AND JUNG-WOOK PARK[1], (Senior Member, IEEE)

[1]School of Electrical and Electronic Engineering, Yonsei University, Seoul 03722, South Korea
[2]Division of Converged Electronic Engineering, Cheongju University, Cheongju 28503, South Korea

Corresponding authors: Donghee Choi (heechoi@cju.ac.kr) and Jung-Wook Park (jungpark@yonsei.ac.kr)

This work was supported in part by the Korea Electric Power Corporation under Grant R22XO02-21, and in part by the National Research Foundation (NRF) funded by the Ministry of Science and ICT (MSIT), South Korea under Grant 2020R1A3B2079407.

ABSTRACT This paper proposes a new coordinated control for multiple wind power plants (WPPs) based on two stepwise inertial control (SIC) methods to effectively release the kinetic energy of the permanent magnet synchronous generators (PMSGs) and improve their inertial response. When a large disturbance occurs, the conventional SIC method increases the output power from the PMSG instantly to arrest the frequency nadir (FN). However, in low wind speed conditions, it may not be able to provide a sufficient inertial response. Therefore, the proposed coordinated control applies the new SIC method to some WPPs by decreasing the output power from their PMSGs for a short period before increasing it. This results in initially accelerating the rotor speed of the PMSGs and reserving their releasable kinetic energy. This means that they are ready to extract more powers without causing the over-deceleration (OD) problem. Also, the proper selection of two SIC methods for multiple WPPs is able to prevent the rate of change of frequency (RoCoF) from increasing. The effectiveness of the proposed coordinated control is verified with several case studies on the IEEE benchmark 39-bus test system. The results show that it effectively improves the frequency stability of the power system without raising the RoCoF in various conditions. Moreover, this enhancement becomes more apparent when the penetration level of wind power is high.

INDEX TERMS Coordinated control, frequency nadir, frequency stability, penetration level of wind power, rate of change of frequency, rotor speed, stepwise inertial control.

I. INTRODUCTION

Frequency is an important index to evaluate the stability of a power system due to a large event. In particular, there are two points to analyze in the dynamic response of frequency. One is the frequency nadir (FN), which is the lowest frequency point during the transient state. The other is the settling frequency. Note that the automatic generation control is activated to recover the system frequency to its nominal value from the settling frequency.

To secure the frequency stability of the power system, the governors of the conventional synchronous generators (SGs) handle the primary frequency control [1]. Thus, when they are replaced with distributed generators (DGs) based on renewable energies such as photovoltaic and wind, etc., it is crucial to take the appropriate control actions for the DGs and energy storage system (ESS) to maintain frequency stability. In particular, many studies have developed novel control methods for ESS to provide fast active power response and enhance power system inertia to secure frequency stability problems [2], [3], [4]. Also, virtual synchronous generators (VSG) have been proposed in many studies to provide similar frequency and inertia responses to support frequency stability [5], [6], [7].

The most widely used control method for the permanent magnet synchronous generator (PMSG) is the maximum power point tracking (MPPT) control method [8], [9]. However, because it does not participate in the frequency support of the system, it can aggravate the frequency stability when a large disturbance occurs. Moreover, as the penetration

The associate editor coordinating the review of this manuscript and approving it for publication was Feng Wu.

level of wind power (PLW) increases, this adverse impact will become more severe [10], [11], [12]. To overcome this problem, the PMSGs are required to provide the appropriate ancillary services with respect to frequency support [13]. The inertial control of PMSGs is a good example.

There are two representative inertial control methods for the PMSGs. One is the frequency-based inertial control (FBIC) method [14], [15], [16], [17], and the other is the stepwise inertial control (SIC) method [18], [19], [21]. The former uses the droop control with the rate of change in frequency and its deviation signals. On the other hand, the latter utilizes the rapid change of active power. In other words, the FBIC method is dependent on the system frequency, whereas the SIC method is independent of it. Therefore, it can be preferably used for more applications. Several SIC methods have been reported to increase the frequency stability with a focus on the FN [19], [20], [21]. They are implemented in the deceleration and acceleration stages. In the former stage, the PMSG releases more power to arrest the FN higher. In contrast, it decreases the power while resulting in a return to the MPPT control method in the latter stage. In particular, the study in [20] sharply increases the output power from the PMSG up to its torque limit, and it decreases the power while considering its minimum speed limit. However, because the power already reaches the torque limit, it needs to decrease the output power before arresting the FN rather than keep releasing it. This results in a late response to arrest the FN even though a large amount of real power is supplied from the PMSGs. Moreover, this problem becomes worse when the PLW is high. To figure it out, the research in [21] initially increases the output power by considering the releasable kinetic energy, and thereafter it maintains the increased power until the FN is arrested. This helps to raise the FN higher, and therefore it improves the frequency stability further. Moreover, instead of newly developing a controller, recent studies have focused on how to apply existing inertial control methods more effectively to multiple wind power plants (WPPs) [22], [23], [24]. Nevertheless, there are no solutions for still maintaining their performance at low wind speeds. This means that the releasable kinetic energy of PMSGs is temporarily insufficient in this low wind speed condition to provide the additional powers to arrest the FN.

To improve the inertial response of multiple WPPs in entire operating conditions (including at low wind speeds), this paper proposes a new SIC method by instantly decreasing the output power for a short period right after detecting a disturbance. This results in accelerating the rotor speed of PMSGs. In other words, it adds the supplementary acceleration stage at the beginning of control before arresting the FN. This enables reserving the releasable kinetic energy of WPPs momentarily. Thus, it can extract more powers than the conventional SIC methods. Moreover, when it is increasing the power to arrest the FN (the rotor speed is therefore decreasing), the risk of over-deceleration (OD) problem can be avoided because the rotor speed is already raised in the supplementary acceleration stage. In summary, the new SIC method can arrest the FN more effectively and efficiently than the conventional SIC methods while therefore improving the frequency stability. On the other hand, initially decreasing the output power from the PMSGs might cause to increase the rate of change of frequency (RoCoF), while resulting in a severe impact [25]. Moreover, this problem becomes critical in the power system with low inertia. Therefore, the proposed coordinated control properly combines the new SIC method with the conventional one for multiple WPPs not to increase the RoCoF while still providing an effective inertial response. The major contributions of this paper are summarized as follows:

- The drawbacks of the conventional inertial control methods for low wind speed conditions have been analyzed.
- A supplementary acceleration stage has been added for the new SIC method to improve the inertial control capability of the wind generator. Therefore, this new method is able to provide larger frequency stability support than conventional SIC methods.
- Coordinated control for multiple WPPs based on conventional and new SIC methods has been proposed to improve FN while considering high RoCoF prevention.
- The proposed coordinated control with the new SIC method operates the multiple WPPs to improve the frequency stability for various PLW and wind conditions, and its efficiency has been verified under various PLW and wind speed conditions using DIgSILENT PowerFactory® software.

This paper is organized as follows. In Section II, the new SIC method for PMSGs is explained in detail with the theoretical analysis. Section III proposes the coordinated control for multiple WPPs by properly selecting two SIC (proposed and conventional) methods. Then, several case studies on the IEEE benchmark 39-bus test system are carried out in Section IV with the DIgSILENT PowerFactory® software [26]. In particular, its performances on various wind speeds and PLWs are compared with those by the MPPT and only conventional SIC methods. Finally, conclusion and future work are given in Section V.

II. TWO STEPWISE INERTIAL CONTROL METHODS

As mentioned previously, two SIC methods are effectively combined by the proposed coordinated control. The first adopts the existing method in [21] (which initially increases the output power from the PMSGs), and the second is newly proposed for this study by providing the supplementary acceleration stage, which initially decreases the output power from the PMSGs.

The structure of PMSG is shown in Fig. 1. It consists of the rotor-side converter (RSC) and grid-side converter (GSC). In this study, the active power is controlled by using the RSC, whereas the DC-link voltage and reactive power are regulated by the GSC. The mechanical power, P_m obtained from wind

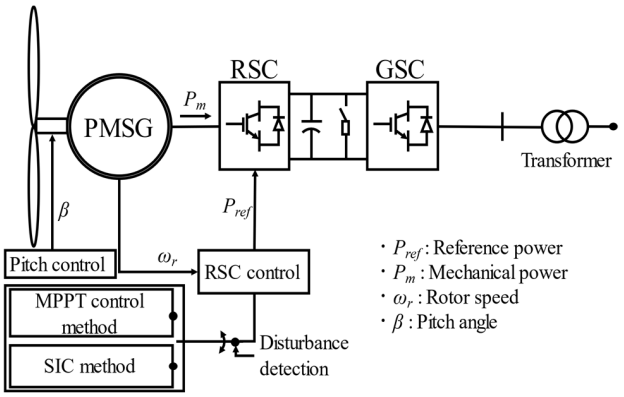

FIGURE 1. Structure of PMSG.

TABLE 1. PMSG parameters.

Parameter	Value
Rated power capacity	2.3 MW
Rated stator voltage	3.3 kV
Nominal frequency	60 Hz
Inertia constant (H)	6 s
Rated wind speed	10.7 m/s
Cut-in wind speed	4 m/s
Cut-out wind speed	24 m/s

is calculated [20] as

$$P_m = \frac{1}{2}\rho\pi r^2 {v_w}^3 c_P(\lambda_{tip}, \beta) \quad (1)$$

where ρ is the air density, r is the rotor radius, v_w is the wind speed, c_P is the power coefficient, λ_{tip} is the tip speed ratio, and β is the pitch angle. When the rotor speed is in the ranges from lower to upper speed limit, which are 0.7 pu and 1.25 pu, respectively, β is maintained to 0° by the pitch control. Then, c_P in (1) is only related to λ_{tip}, and it has the maximum value when λ_{tip} is optimally selected by the MPPT control method [27]. The parameter specifications of PMSG are given in Table 1.

A. SIC METHOD-1

Like the other conventional SIC methods, the SIC method-1 increases the power right after detecting a disturbance. In particular, this increased power is maintained until the FN is arrested, as shown in Fig. 2. The increased power by the SIC method-1, $\Delta P_{\mathrm{SIC}-1}$ is calculated [21] as

$$\Delta P_{\mathrm{SIC}-1} = [P_{T-\mathrm{lim}}(\omega_0) - P_0] \cdot (\omega_0^n - \omega_{\mathrm{min}}^n) \quad (2)$$

where P_0 and ω_0 are the initial output power from the PMSG and steady-state rotor speed before a disturbance occurs, respectively. ω_{min} is the minimum speed limit, $P_{T-\mathrm{lim}}(\omega_0)$ is the power referring to the torque limit at ω_0, and superscript n is the parameter depending on the PLW. Because the power is maintained after it is increased by (2), this supports the frequency stability with the other SGs, which have a relatively late response. As the result, the FN can be raised higher. After arresting the FN, the active power is decreased (see the dash-dotted blue trajectory in Figs. 2 and 3(a)). Then, the rotor speed (ω_r) is recovered to ω_0 so as to generate the maximum power in the MPPT curve (which is indicated by the dotted green line in Fig. 2). If $\Delta P_{\mathrm{SIC}-1}$ in (2) is excessive during the arresting period of FN, the amount of decrease in the active power and its decreasing rate also become high. This means that the other SGs with a relatively late response are required to compensate for the decreased power. Thus, this can cause more decline in the FN while making the frequency response late. Moreover, the OD problem is subject to occur in the region of low ω_0. To solve this problem, the value of the term in the second bracket or n in (2) needs to be small to reduce $\Delta P_{\mathrm{SIC}-1}$. This means that the SIC method-1 enables the PMSG to provide effective frequency support at high wind speeds. However, it is difficult to do so in low wind speed conditions.

B. NEWLY PROPOSED SIC METHOD-2

The operational characteristic of the proposed SIC method-2 is represented by the thick-solid red trajectory on the plane of power versus rotor speed in Fig. 2. The corresponding time-domain characteristic is also shown in Fig. 3(b). Again, the SIC method-1 increases the power right after detecting a disturbance in the power system. However, the FN is not arrested as soon as the disturbance occurs. Instead, it takes about a few seconds to arrest the FN [1]. Therefore, the proposed SIC method-2 adds the new step of stage I (from point A to B in Figs. 2 and 3(b)) to accelerate ω_r. This can reserve the releasable kinetic energy of PMSGs such that they are ready to extract more power to arrest the FN higher without causing ω_r to decrease dramatically. As the result, the SIC method-2 is particularly useful in low wind speed conditions to provide an effective inertial response. The detailed operations in six stages for the SIC method-2 are explained below.

1) *Stage I – Reserving the Releasable Kinetic Energy:* The first stage of the proposed method aims to reserve the releasable kinetic energy of PMSGs as a disturbance occurs. To do so, the SIC method-2 starts to accelerate ω_r by decreasing the reference power for the PMSG, P_{ref}, as

$$P_{ref}(t) = P_0 - \Delta P_{SIC-2}^{\mathrm{A}}, \quad \text{for } t_0 \leqslant t < t_{\mathrm{B}} \quad (3)$$

where t_{B} is the time period to accelerate ω_r from ω_0 to ω_{B}. Meanwhile, P_{ref} is firstly decreased at t_0, and thereafter it is maintained for t_{B} (from point A' to B in Figs. 2 and 3(b)). The period of stage I is short because the PMSG must increase the power in later stages. Normally, as the FN occurs around 5 s to 10 s after a disturbance occurs, t_{B} is set to the short period of 1 s, which is sufficient for the PMSG to reserve additional releasable kinetic energy without disturbing the later stages.

$\Delta P_{\mathrm{SIC}-2}^{\mathrm{A}}$ in (3) is set by considering the current stored kinetic energy of the PMSG. In the region of high ω_0, it has sufficient kinetic energy. Thus, the relatively small $\Delta P_{\mathrm{SIC}-2}^{\mathrm{A}}$ can be used. In contrast, because it has low kinetic energy

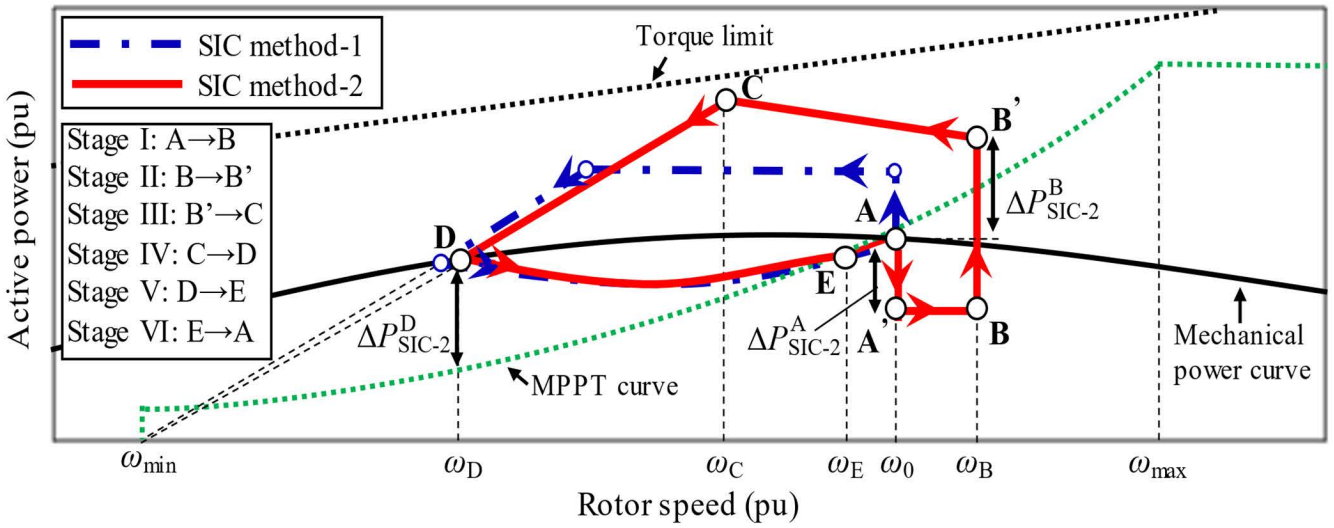

FIGURE 2. Comparison of operational characteristics by two SIC methods on the plane of power versus rotor speed.

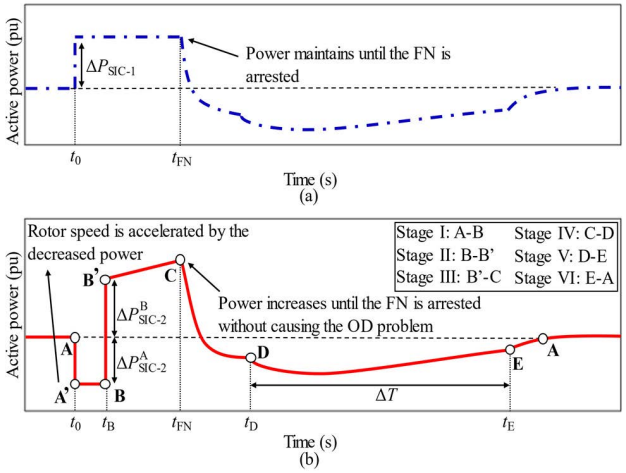

FIGURE 3. Operational characteristic in time-domain by (a) SIC method-1, (b) SIC method-2.

in the region of low ω_0 (low wind speed conditions), the large value of ΔP^{A}_{SIC-2} is selected. In particular, ω_r cannot be beyond the maximum speed limit, ω_{max}. Then, ΔP^{A}_{SIC-2} is determined as

$$\Delta P^{A}_{SIC-2} = P_0 \cdot \frac{\omega_{max} - \omega_0}{H\omega_0^2} \cdot k \quad (4)$$

where k is the constant that considers the inertia of the power system. When a system has large inertia, the power decrement of ΔP^{A}_{SIC-2} will not cause the RoCoF problem. However, it becomes serious for the power system with low inertia. Thereby, the smaller ΔP^{A}_{SIC-2} must be decreased from the PMSG. Note that the system inertia constant of the IEEE benchmark 39-bus test system is about 4.5 s, and k is set to 4. In addition, the RoCoF problem is further solved by the proposed coordinated control described in the next section.

2) *Stage II – Preparing to Arrest the FN:* In this stage, the proposed SIC method initially increases P_{ref} to support the frequency stability similar to that of the SIC method-1. However, since the power is increased after the rotor speed is accelerated, the power increment in this stage (ΔP^{B}_{SIC-2}) is higher than ΔP_{SIC-1}. Thus, it is calculated at ω_B (after the acceleration of ω_r is carried out in stage I) as

$$P_{ref}(t) = P_0 + \Delta P^{B}_{SIC-2} \text{ at } t = t_B, \quad (5)$$

$$\Delta P^{B}_{SIC-2} = [P_{T-lim}(\omega_B) - P_0] \cdot (\omega_B^n - \omega_{min}^n) \quad (6)$$

where $P_{T-lim}(\omega_B)$ is the power referring to the torque limit at ω_B. Again, if ΔP_{SIC-1} and ΔP^{B}_{SIC-2} are excessive, this can cause other SGs to compensate for the decreased power at stage IV, while resulting in more decline of the FN. Therefore, the values of n in (2) and (6) are set to 1.35, 0.75, and 0.5 when the overall PLWs are 20%, 40%, and 60%, respectively, for this study.

3) *Stage III – Arresting the FN:* This stage aims to arrest the FN at the highest. As mentioned previously, the power is maintained by the SIC method-1 until the FN is arrested. In contrast, the SIC method-2 keeps increasing power steadily with the releasable kinetic energy obtained in stage I until the FN is arrested as

$$P_{ref}(t) = R \cdot (t - t_{B'}) + P_{ref}(t_{B'}), \quad \text{for } t_{B'} < t \leqslant t_{FN} \quad (7)$$

where R is the slope of the line from point B' to C in Fig. 3(b). If its value is high, the support for arresting the FN is reinforced by extracting more power. However, when it is too excessive, P_{ref} increases extremely, causing ω_r to decrease dramatically. This study focuses on extracting more additional power by the SIC method-2 than the SIC method-1 without decreasing the lowest value of ω_r (preventing the OD problem). Based on many simulation studies in various

conditions, the value of R is set to 0.02, 0.013, and 0.01 when the overall PLWs are 20%, 40%, and 60%, respectively.

4) *Stage IV – Preparing Acceleration for Recovery:* After providing frequency support in previous stages, this stage ensures that ω_r can recover back to ω_0, at which the MPPT control method is applied back. To do so, ω_D at point D, where P_m and P_{ref} are the same, must be greater than ω_{min}. Then, P_{ref} is computed by

$$P_{ref}(\omega_r) = \frac{P_{ref}(\omega_C)}{\omega_C - \omega_{\min}} \cdot (\omega_r - \omega_{\min}), \quad \text{for } \omega_D \leqslant \omega_r < \omega_C \tag{8}$$

Because P_{ref} is less than P_m after point D, ω_r starts to accelerate to ω_0 in the next stage.

5) *Stages V and VI – Accelerating Back to the MPPT Control Method:* After implementing the SIC method-2 in these stages, the PMSG will be operated in the MPPT control method. In particular, the following two issues are emphasized in these stages. First, a second frequency dip must be prevented while recovering to the MPPT control method. Second, the time period in stage V (from point D to E) of returning to the MPPT control method must be short for the case of further disturbance. Then, P_{ref} in stage V is obtained as

$$P_{ref}(\omega_r, t) = k_{opt}\omega_r{}^3 + \Delta P^{D}_{SIC-2}\left(-\frac{1}{\Delta T}(t - t_D) + 1\right), \quad \text{for } \omega_D < \omega_r \leqslant \omega_E \tag{9}$$

where ΔP^{D}_{SIC-2} is the power difference between P_{ref} and the power of the MPPT curve at ω_D (see Fig. 2), and ΔT is the time interval of points D and E (see Fig. 3(b)). The small value of ΔT gives the fast recovery to stage VI, in which the MPPT control method is used. However, the second frequency dip can occur because it might cause to excessively decrease P_{ref}. In contrast, the large value of ΔT slows the recovery, whereas it prevents the second frequency dip. In this study, ΔT is set to 15 s, 25 s, and 35 s when the overall PLWs are 20%, 40%, and 60%, respectively.

In summary, the proposed SIC method-2 is able to increase P_{ref} more (in stages II and III) than the conventional SIC methods after accelerating ω_r (in stage I), which prevents causing the excessive decreasing rate in P_{ref} after arresting the FN and OD problem.

III. PROPOSED COORDINATED CONTROL FOR MULTIPLE WPPS

As mentioned previously, even though the SIC method-2 is able to extract more power than the SIC method-1, the initially decreased power in stage I may increase the RoCoF. Thus, to avoid this, the proposed coordinated control newly determines the operation of multiple WPPs in one of two SIC methods. To do so, the objective function, J is firstly formulated to maximize the inertial response from all WPPs with the constraint of preventing the high RoCoF as

$$J = \max\left\{\sum_{j=1}^{M} \mathrm{WPP}_{IR,j}\left(v_{w,j}, S_j\right)\right\}$$
$$s.t. \quad \sum_{j=1}^{M} \mathrm{WPP}_{init,j}\left(v_{w,j}, S_j\right) \geqslant 0 \tag{10}$$

where v_w and S are the wind speed and power capacity of WPP, respectively, and M is the total number of WPPs. Also, the inertial response (WPP_{IR}) and initial power change (WPP_{init}) of WPP are defined as

$$\mathrm{WPP}_{IR}(v_w, S) = \begin{cases} \Delta P_{SIC-1} & \text{if WPP is operated in SIC method} - 1 \\ \Delta P^{B}_{SIC-2} & \text{if WPP is operated in SIC method} - 2 \end{cases} \tag{11}$$

$$\mathrm{WPP}_{init}(v_w, S) = \begin{cases} S \cdot \Delta P_{SIC-1} & \text{if WPP is operated in SIC method} - 1 \\ -S \cdot \Delta P^{A}_{SIC-2} & \text{if WPP is operated in SIC method} - 2 \end{cases} \tag{12}$$

According to various wind conditions, the releasable kinetic energy required for the inertial response of each WPP is different. In order to maximize J in (10) with the given constraint, the SIC method-2 is mostly applied to the WPPs, which can effectively increase their releasable kinetic energy in stage I. On the other hand, the SIC method-1 is applied to the WPPs with the least effect in the supplementary acceleration stage. This is because if the WPPs already have sufficient releasable kinetic energy, stage I of the SIC method-2 will only worsen the risk of increasing the RoCoF. The difference in power increment between two SIC methods for each WPP, P_{dif}, is defined as

$$P_{dif} = \Delta P^{B}_{SIC-2} - \Delta P_{SIC-1} \tag{13}$$

If the value of P_{dif} is high, it means that the WPPs can reserve enough releasable kinetic energy in stage I by the SIC method-2. Particularly when the WPPs have a small releasable kinetic energy at low wind speeds, the SIC method-2 is very effective for increasing their inertial control capability. As the result, it is preferably applied to the WPPs with high P_{dif}. In contrast, the WPPs with low P_{dif} already have sufficient releasable kinetic energy. Thus, they need to increase their power outputs by the SIC method-1 to compensate for the decreased power from the other WPPs (by the SIC method-2) during stage I. Finally, the function J in (10) can be modified for this study as

$$J = \max\left(\sum_{j=1}^{M}\left\{P_{dif,j}\underline{\mathbf{x}}(j)\right\}\right)$$
$$s.t. \quad \sum_{j=1}^{M}\left\{S_j\Delta P_{SIC-1,j}\left[\sim \underline{\mathbf{x}}(j)\right] - S_j\Delta P^{A}_{SIC-2,j}\underline{\mathbf{x}}(j)\right\} \geqslant 0 \tag{14}$$

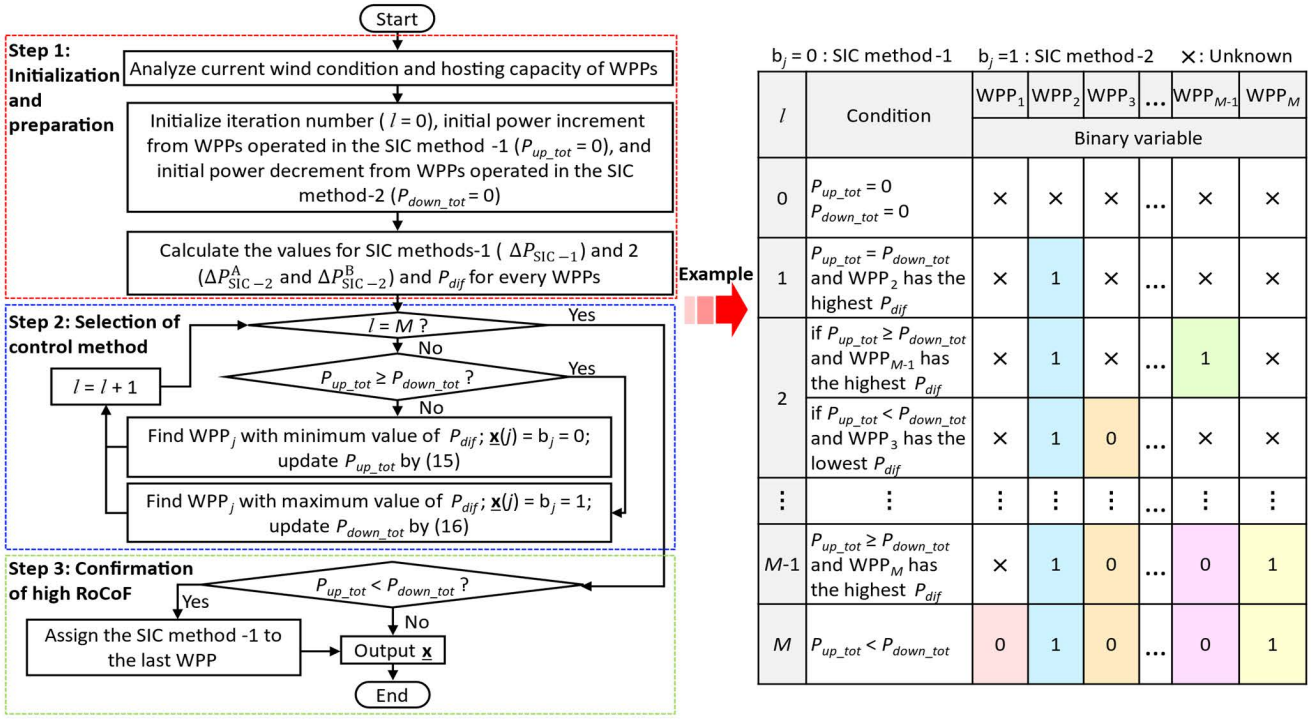

l	Condition	WPP$_1$	WPP$_2$	WPP$_3$	...	WPP$_{M-1}$	WPP$_M$
		Binary variable					
0	$P_{up\_tot} = 0$ $P_{down\_tot} = 0$	×	×	×	...	×	×
1	$P_{up\_tot} = P_{down\_tot}$ and WPP$_2$ has the highest P_{dif}	×	1	×	...	×	×
2	if $P_{up\_tot} \geq P_{down\_tot}$ and WPP$_{M-1}$ has the highest P_{dif}	×	1	×	...	1	×
	if $P_{up\_tot} < P_{down\_tot}$ and WPP$_3$ has the lowest P_{dif}	×	1	0	...	×	×
⋮	⋮	⋮	⋮	⋮	...	⋮	⋮
M-1	$P_{up\_tot} \geq P_{down\_tot}$ and WPP$_M$ has the highest P_{dif}	×	1	0	...	0	1
M	$P_{up\_tot} < P_{down\_tot}$	0	1	0	...	0	1

FIGURE 4. Flowchart to implement the proposed coordinated control for multiple WPPs.

where the vector $\underline{\mathbf{x}} = [b_1, b_2, \ldots, b_N]^t$ is formed with binary variables, b_j. Note that if b_j is 0, the WPP$_j$ operates by the SIC method-1. In contrast, if b_j is 1, it operates by the SIC method-2. The bitwise NOT operation, $\sim$ in (14) denotes inverting the value of b_j from 0 to 1, or vice versa. Then, the proposed coordinated control for multiple WPPs is implemented as shown in Fig. 4, while maximizing the value of J in (14). Firstly, the variables, v_w, S, N, and l (number of iterations) are initially defined. Also, $P_{up\ tot}$ and P_{down_tot} are defined as the total power initially increased and decreased by the WPPs operated in the SIC methods 1 and 2, respectively. Their values are initially set to zero, and they are updated in every iteration during the decision process as

$$P_{up\_tot} = P_{up\_tot} + S_j \Delta P_{\mathrm{SIC}-1,j} \tag{15}$$

$$P_{down\_tot} = P_{down\_tot} + S_j \Delta P^{A}_{\mathrm{SIC}-2,j} \tag{16}$$

Thereafter, $\Delta P_{\mathrm{SIC}-1}$, $\Delta P^{\mathrm{A}}_{\mathrm{SIC}-2}$, and $\Delta P^{\mathrm{B}}_{\mathrm{SIC}-2}$ are computed for all WPPs by (2), (4), and (6), respectively. While considering the prevention of high RoCoF, step 2 in Fig. 4 starts to process in the first iteration by firstly assigning the SIC method-2 to the WPP with the highest value of P_{dif} in (13) among all WPPs (therefore maximizing J). From the next iteration, if the value of P_{up_tot} becomes lower than P_{down_tot}, the SIC method-1 is applied to the WPP with the lowest value of P_{dif} in (13) among the remaining WPPs except for the WPPs selected in the previous iteration. Again, as the WPP with the lower value of P_{dif} already has sufficient releasable kinetic energy, it should be operated in the SIC method-1 to prevent the high RoCoF. On the other hand, if the value of P_{up_tot} becomes higher than P_{down_tot}, the SIC method-2 is applied to the WPP with the highest value of P_{dif}. This decision process is repeated until l reaches N.

When l is equal to M, the value of P_{down_tot} might be larger than that of P_{up_tot} due to the last WPP assigned by the SIC method-2. For this case, the SIC method-2 must be switched to SIC method-1 for this WPP to prevent the high RoCoF in step 3 of Fig. 4. Finally, the output $\underline{\mathbf{x}}$ represents the final selection of SIC methods 1 and 2 for all WPPs such that it provides the most effective dynamic frequency response without increasing the RoCoF in stage I.

An example of the flowchart process is also given in Fig. 4. As shown in the figure, P_{up_tot} and P_{down_tot} are initialized when l is 0. In the next iteration ($l = 1$), since the value of P_{up_tot} is equal to P_{down_tot}, SIC method-2 is assigned to WPP with the highest P_{dif}, which is WPP$_2$. Thereafter, until l reaches M, if the value of P_{down_tot} becomes higher than P_{up_tot}, SIC method-1 is assigned to WPP with the lowest P_{dif}. In contrast, SIC method-2 is assigned to WPP with the highest P_{dif} if P_{up_tot} remains higher than P_{down_tot}. At the last iteration ($l = M$) if the value of P_{down_tot} is larger than that of P_{up_tot} due to the last WPP assigned by the SIC method-2, this WPP is switched to SIC method-1 to prevent the high RoCoF.

IV. SIMULATION RESULTS

To evaluate the performance of proposed coordinated control, several case studies are carried out on the IEEE benchmark 39-bus test system [28] in Fig. 5 with various v_w (of 7 m/s and

TABLE 2. Test conditions used for case studies.

Case	Area 2		Area 3		Area 4		Overall PLW (%)
	v_w (m/s)	PLW (%)	v_w (m/s)	PLW (%)	v_w (m/s)	PLW (%)	
1	7	3.2	8.5	6.8	7	10	20
2	7	6.5	8.5	13.5	7	20	40
3	7	9.7	8.5	20.3	7	30	60

TABLE 3. Parameters used for case studies.

	Case 1		Case 2		Case 3	
	PLW - 20%		PLW - 40%		PLW - 60%	
	v_w - 7 m/s	v_w - 8.5 m/s	v_w - 7 m/s	v_w - 8.5 m/s	v_w - 7 m/s	v_w - 8.5 m/s
P_0 (pu)	0.28	0.5	0.28	0.5	0.28	0.5
ω_0 (pu)	0.82	0.997	0.82	0.997	0.82	0.997
$\Delta P_{\text{SIC}-1}$ (pu)	0.07	0.156	0.046	0.096	0.033	0.067
$\Delta P^{\text{A}}_{\text{SIC}-2}$ (pu)	0.12	0.087	0.12	0.087	0.12	0.087
$\Delta P^{\text{B}}_{\text{SIC}-2}$ (pu)	0.087	0.165	0.052	0.101	0.037	0.07

TABLE 4. Output powers from SGs and WPPs before a disturbance occurs.

Case	Output power (MW)									
	SG_1	SG_2	SG_3	SG_4	SG_5	SG_6	SG_7	SG_8	SG_9	SG_{10}
1	780	500	440	480	470	483	-	565	610	670
2	780	500	480	480	-	483	-	620	620	670
3	780	600	-	622	-	423	-	528	630	670
	WPP_1	WPP_2	WPP_3	WPP_4	WPP_5	WPP_6	WPP_7	WPP_8		
1	19	29	40	57	82	64	46	38		
2	38	57	80	114	165	128	92	77		
3	57	86	120	171	247	192	138	115		

8.5 m/s) and PLWs (of 20%, 40%, and 60%). In particular, the frequency stability improvement by the proposed coordinated controlis compared with that of the MPPT control and conventional SIC method in [20] for each case study. The PLW [21] is defined as the ratio of the total installed capacity of WPPs and total load, which is 5337 MW in this study. Table 2 shows the test conditions of three cases according to different v_w and PLW. Correspondingly, the output powers from all SGs and WPPs for three cases are given in Table 4 before SG_{10} is suddenly disconnected at 15 s.

A. CASE 1 WITH WIND SPEED OF 7 m/S AND 8.5 m/S -OVERALL PLW OF 20%

When v_w is 7 m/s, the initial values for releasable kinetic energy, ω_0, and output power from WPPs are 1.1 s (it is calculated by $H(\omega_0^2 - \omega_{\min}^2)$ [29]), 0.82 pu, and 0.28 pu, respectively. On the other hand, when v_w is 8.5 m/s, the initial values of releasable kinetic energy, ω_0, and output power for WPPs are 3.02 s, 0.997 pu, and 0.5 pu, respectively. For WPPs with v_w of 7 m/s, it is shown that P_{ref} is increased from 0.28 pu to 0.73 pu at maximum, and it is then decreased during the FN arrestment when the conventional SIC method is applied. However, by the SIC method-1, P_{ref} is increased

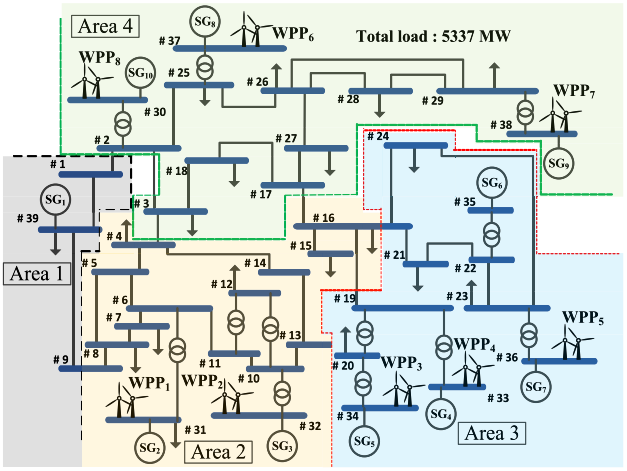

FIGURE 5. IEEE 39-bus test system with eight WPPs.

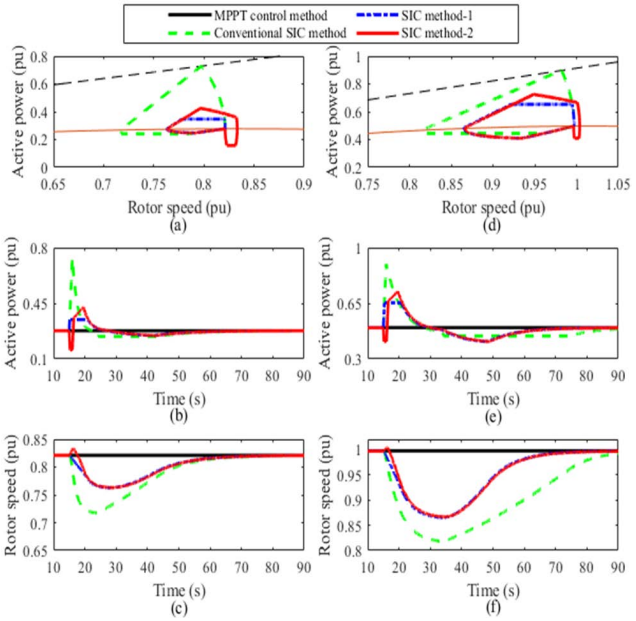

FIGURE 6. Comparison results for case 1: (a) Trajectories on the plane of P_{ref} versus ω_r for WPPs with v_w of 7 m/s, (b) Output power from WPPs with v_w of 7 m/s, (c) Rotor speed of WPPs with v_w of 7 m/s, (d) Trajectories on the plane of P_{ref} versus ω_r for WPPs with v_w of 8.5 m/s, (e) Output power from WPPs with v_w of 8.5 m/s, (f) Rotor speed of WPPs with v_w of 8.5 m/s.

up to only 0.35 pu by (2). Thereafter, it is maintained until the FN is arrested. In contrast, when the SIC method-2 is applied, P_{ref} is initially decreased by 0.12 pu by (4). Thereby, ω_r is slightly accelerated from 0.82 pu to 0.83 pu while increasing the releasable kinetic energy from 1.1 s to 1.2 s. Then, P_{ref} is increased to 0.36 pu by (5), and it is kept increasing steadily by (7) until the FN is arrested. Also, it is observed from Fig. 6(c) that the lowest value of ω_r drops to 0.72 pu by the conventional SIC method. On the contrary, it drops to 0.76 pu by the SIC methods 1 and 2. This clearly verifies that the SIC method-2 avoids the risk of OD problem effectively even though it produces more power than the SIC method-1.

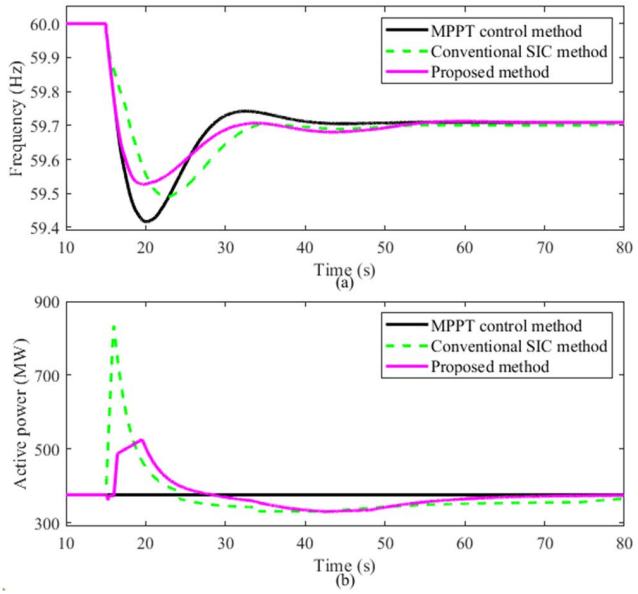

FIGURE 7. Results of case 1. (a) System frequency, (b) Total output power from WPPs.

In contrast, for WPPs with v_w of 8.5 m/s, the conventional SIC method increases P_{ref} from 0.5 pu to 0.89 pu at maximum, and it is then decreased during the FN arrestment. Because ω_0 is higher than that of WPPs with v_w of 7 m/s, the decreasing rate of P_{ref} becomes smaller. This means that the defective impact of the conventional SIC method on the FN can be relieved to a certain degree when ω_0 is relatively high. For the SIC method-1, P_{ref} is increased up to 0.65 pu by (2), and it is maintained until the FN is arrested. On the contrary, the SIC method-2 initially decreases P_{ref} by 0.087 pu according to (4). As the result, ω_r is accelerated to 1.004 pu, and the releasable kinetic energy is increased to 3.11 s. Thereafter, P_{ref} is increased to 0.66 pu by (5), and it is kept increasing by (7) until the FN is arrested.

Next, $\underline{\mathbf{x}}$ is determined by the flowchart shown in Fig. 4 such that $\Delta P_{\mathrm{SIC}-1}$, $\Delta P^{\mathrm{A}}_{\mathrm{SIC}-2}$, and $\Delta P^{\mathrm{B}}_{\mathrm{SIC}-2}$ are 0.07 pu, 0.12 pu, and 0.08 pu for WPPs with v_w of 7 m/s, and 0.156 pu, 0.087 pu, and 0.165 pu for WPPs with v_w of 8.5 m/s, respectively. As mentioned in Section III, the kinetic energy is sufficient in the region of high ω_0 when compared to the region of low ω_0. Thus, the SIC method-2 is preferably applied to WPPs in Areas 2 and 4, which is in the region of low ω_0. As the result, while the SIC method-2 is applied to four WPPs (WPP_1, WPP_2, WPP_6, and WPP_7), the SIC method-1 is applied to the other WPPs (WPP_3, WPP_4, WPP_5, and WPP_8).

The results are shown in Fig. 7. It is observed that the total output power from WPPs is maintained at about 375 MW during stage I. This is because $\Delta P_{\mathrm{SIC}-1}$ and $\Delta P^{\mathrm{A}}_{\mathrm{SIC}-2}$ are compensated. Also, the corresponding maximum RoCoF is kept to 1.83 Hz/s, which is the same as the case by applying the MPPT control method. Also, it arrests the FN at 59.53 Hz, which is higher than the MPPT control and conventional SIC methods by 0.11 Hz and 0.04 Hz, respectively. When the conventional SIC method is applied, it is shown that the total output power from WPPs is dramatically increased, and then it is decreased before the FN is arrested. Therefore, it operates the governors of other SGs with a relatively late response to compensate for power. This results in causing more decline in the FN (see Fig. 7(a)) while making the frequency response late. In other words, it delays the time occurrence of FN by 2.58 s than the MPPT control method with 20.06 s. In contrast, the proposed method arrests the FN faster by 0.34 s than the MPPT control method. As the result, it is clearly observed from Fig. 7(a) that it enables to arrest the FN highest and fastest without increasing the RoCoF.

B. CASE 2 WITH WIND SPEED OF 7 m/S AND 8.5 m/S -OVERALL PLW OF 40%

For this case study, v_w is kept to 7 m/s (for Areas 2 and 4) and 8.5 m/s (for Area 3) like case 1. The only overall PLW is increased from 20% to 40%. Therefore, the initial values of releasable kinetic energy, ω_0, and output power from WPPs are the same as those in case 1. The system responses by the MPPT control and conventional SIC methods are not changed even though the overall PLW is increased twice. For the SIC method-1, the WPPs with v_w of 7 m/s and 8.5 m/s increase P_{ref} by 0.046 pu and 0.096 pu, respectively. They are lower than those of case 1. This is because the value of n in (2) becomes smaller from 1.35 to 0.75. When the SIC method-2 is applied, the value of n in (6) is changed from 1.35 to 0.75 in stage II. Thus, P_{ref} of WPPs with v_w of 7 m/s and 8.5 m/s are increased by 0.052 pu and 0.101 pu, respectively. They are also smaller than those of case 1. Thereafter, P_{ref} is kept increasing steadily by (7) until the FN is arrested.

Then, the proposed coordinated control is applied as follows. While $\Delta P^{\mathrm{A}}_{\mathrm{SIC}-2}$ is maintained at 0.12 pu and 0.087 pu like case 1, respectively, for v_w of 7 m/s and 8 m/s, $\Delta P_{\mathrm{SIC}-1}$ is decreased to 0.046 pu and 0.096 pu, respectively. Moreover, $\Delta P^{\mathrm{B}}_{\mathrm{SIC}-2}$ for v_w of 7 m/s and 8.5 m/s is also decreased to 0.052 pu and 0.101 pu, respectively. Thereafter, five WPPs (WPP_3, WPP_4, WPP_5, WPP_7, and WPP_8) are determined to operate by the SIC method-1 for this case. The other three WPPs (WPP_1, WPP_2, and WPP_6) are operated by the SIC method-2.

The results are shown in Fig. 8. It is observed that the proposed coordinated control maintains the total output power from WPPs to 751 MW during stage I of the SIC method-2. As the result, the proposed method improves the dynamic frequency response most effectively without exceeding the maximum RoCoF when compared to the case when the MPPT control method is applied. In particular, it arrests the FN at 59.49 Hz, which is higher than the MPPT control and conventional SIC methods by 0.15 Hz and 0.11 Hz, respectively. Moreover, the proposed coordinated control arrests the FN most rapidly without increasing the RoCoF. In other words, the time occurrence of FN is faster than the MPPT control and conventional SIC methods by 0.81 s and 5.94 s, respectively. In particular, the defective effect (which

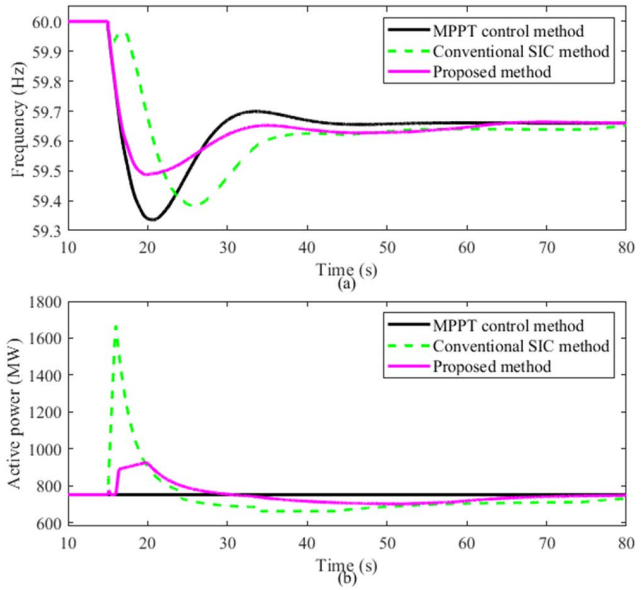

FIGURE 8. Results of case 2. (a) System frequency, (b) Total output power from WPPs.

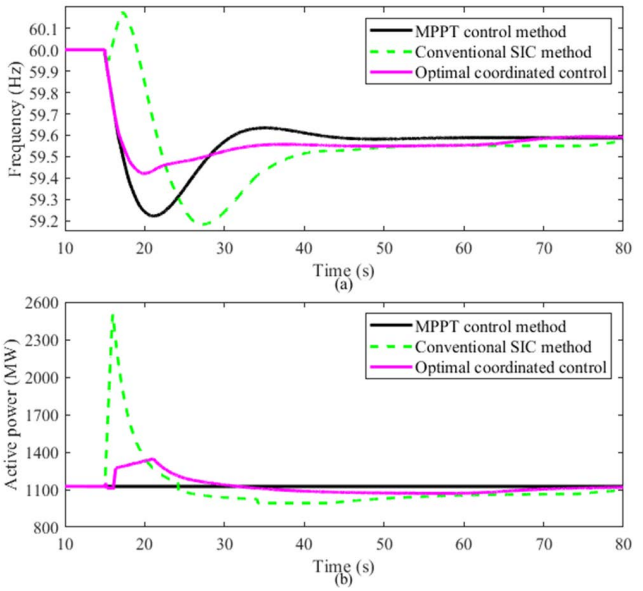

FIGURE 9. Results of case 3 (*N*-1 contingency). (a) System frequency, (b) Total output power from WPPs.

is the late response causing an adverse impact on FN) of the conventional SIC method becomes more severe when the overall PLW is increased. As the result, the frequency support by the conventional SIC method becomes insignificant, and it delays the time occurrence of FN by 5.13 s than the MPPT control method.

C. CASE 3 WITH WIND SPEED OF 7 m/S AND 8.5 m/S -OVERALL PLW OF 60%

In this case, because the PLW is increased to 60%, only $\Delta P_{\mathrm{SIC}-1}$ and $\Delta P^{\mathrm{B}}_{\mathrm{SIC}-2}$ become different. Note that as n in (2) and (6) is changed from 0.75 to 0.5 in stage II, they are decreased to 0.033 pu and 0.037 pu for WPPs with v_w of 7 m/s, and 0.067 pu and 0.07 pu for WPPs with v_w of 8.5 m/s, respectively. Then, five WPPs (WPP_3, WPP_4, WPP_5, WPP_7, and WPP_8) are determined to operate by the SIC method-1, and the other three WPPs (WPP_1, WPP_2, and WPP_6) are operated by the SIC method-2.

The results are shown in Fig. 9. The proposed coordinated control arrests the FN at 59.42 Hz, which is higher than the MPPT control and conventional SIC methods by 0.2 Hz and 0.24 Hz, respectively. This clearly verifies that the proposed method is able to enhance the frequency stability more effectively when the overall PLW is increased. In particular, the excessive power increment from the conventional SIC method causes the frequency to go over the nominal value (which is 60 Hz), and it also causes a severe impact on the FN.

In addition, Fig. 10 shows the results of $N-2$ contingency (SG_6 and SG_8 disconnection). Since the size of the generation loss is larger than $N-1$ contingency, more severe frequency problem is observed. Similar to previous case studies, the proposed coordinated control improves the dynamic frequency

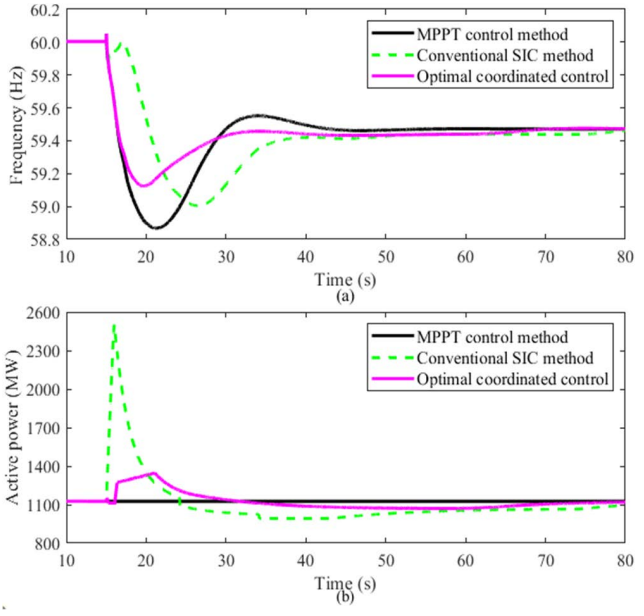

FIGURE 10. Results of case 3 (*N*-2 contingency). (a) System frequency, (b) Total output power from WPPs.

response most effectively without causing RoCoF problem. In particular, it arrests the FN at 59.13 Hz, which is higher than the MPPT control and conventional SIC methods by 0.27 Hz and 0.13 Hz, respectively.

Table 5 summarizes the operation of all WPPs for three case studies. It is observed that the SIC method-2 tends to be assigned to the WPPs (except for the WPP_8) in the low v_w regions. In contrast, the SIC method-1 does in the high v_w regions. Table 6 compares the values of the FN and time occurrence of FN by three methods. It is observed that the

TABLE 5. Overview of WPPs operation in three case studies.

		WPP_1	WPP_2	WPP_3	WPP_4	WPP_5	WPP_6	WPP_7	WPP_8
v_w (m/s)		7	7	8.5	8.5	8.5	7	7	7
S (MW)	Case 1	69	104	81	115	166	230	166	138
	Case 2	138	207	161	230	331	460	331	276
	Case 3	207	311	242	345	497	690	497	414
Type of SIC method	Case 1	2	2	1	1	1	2	2	1
	Case 2	2	2	1	1	1	2	1	1
	Case 3	2	2	1	1	1	2	1	1

TABLE 6. Comparison of performances by three methods.

	Method	Case 1	Case 2	Case 3 (N-1 contingency)	Case 3 (N-2 contingency)
FN (Hz)	MPPT control	59.42	59.34	59.22	58.86
	Conventional SIC	59.49	59.38	59.18	59
	Proposed coordinated control	**59.53**	**59.49**	**59.42**	**59.13**
Time occurrence of FN (s)	MPPT control	20.06	20.65	21.03	21.13
	Conventional SIC	22.64	25.78	27.29	26.52
	Proposed coordinated control	**19.72**	**19.84**	**19.81**	**19.67**

proposed coordinated control improves the frequency stability by arresting the FN most effectively while maintaining the RoCoF. Moreover, it provides better dynamic performance than other methods, particularly when the PLW is increasing.

V. CONCLUSION AND FUTURE WORK

This paper proposed the novel coordinated control for WPPs. It combined two different SIC methods. The first method is the existing SIC method, which increases the power immediately as a disturbance occurs. The other method was newly proposed with a new acceleration stage of rotor speed at the beginning of its control action. This can increase the releasable kinetic energy of PMSG. Also, it enables to extract more real power while effectively avoiding the risk of OD of rotor speed. Therefore, this new method is able to provide a larger inertial response to support frequency stability. However, initially decreased power in the acceleration stage of this method may cause high RoCoF. Thus, the proposed coordinated control properly combines the new SIC method with the conventional one for multiple WPPs so that it improves the dynamic frequency response most effectively without increasing the RoCoF.

The performances of proposed coordinated control were evaluated by several case studies on IEEE benchmark 39-bus test system in various conditions with different wind speeds and PLWs. The results showed that the proposed methodenhances the frequency stability most effectively and efficiently among other control methods. In particular, this improvement becomes clear when the PLW is increased. Thus, it would be expected that the proposed coordinated control is preferably used for the operation of a power system with high PLW.

Furthermore, while the additional releasable kinetic energy obtained by the proposed SIC method was used to support dynamic frequency stability, this additional energy can be used for various frequency responses. Therefore, future work will focus on improving both dynamic and steady-state frequency stabilities.

REFERENCES

[1] J. Eto, J. Undrill, C. Roberts, P. Mackin, and J. Ellis, "Frequency control requirements for reliable interconnection frequency response," Lawrence Berkley Nat. Lab., Berkley, CA, USA, Tech. Rep., 2018, vol. 2001103. [Online]. Available: https://escholarship.org/content/qt0z77p518/qt0z77p518_noSplash_c65afe3169f836a4464351fba782d8ae.pdf

[2] H. Golpira, A. Atarodi, S. Amini, A. R. Messina, B. Francois, and H. Bevrani, "Optimal energy storage system-based virtual inertia placement: A frequency stability point of view," *IEEE Trans. Power Syst.*, vol. 35, no. 6, pp. 4824–4835, Nov. 2020.

[3] C. Zhang, E. Rakhshani, N. Veerakumar, J. L. R. Torres, and P. Palensky, "Modeling and optimal tuning of hybrid ESS supporting fast active power regulation of fully decoupled wind power generators," *IEEE Access*, vol. 9, pp. 46409–46421, 2021.

[4] L. Meng, J. Zafar, S. K. Khadem, A. Collinson, K. C. Murchie, F. Coffele, and G. M. Burt, "Fast frequency response from energy storage systems—A review of grid standards, projects and technical issues," *IEEE Trans. Smart Grid*, vol. 11, no. 2, pp. 1566–1581, Mar. 2020.

[5] A. Fathi, Q. Shafiee, and H. Bevrani, "Robust frequency control of microgrids using an extended virtual synchronous generator," *IEEE Trans. Power Syst.*, vol. 33, no. 6, pp. 6289–6297, Nov. 2018.

[6] K. Shi, H. Ye, W. Song, and G. Zhou, "Virtual inertia control strategy in microgrid based on virtual synchronous generator technology," *IEEE Access*, vol. 6, pp. 27949–27957, 2018.

[7] D. Li, Q. Zhu, S. Lin, and X. Y. Bian, "A self-adaptive inertia and damping combination control of VSG to support frequency stability," *IEEE Trans. Energy Convers.*, vol. 32, no. 1, pp. 397–398, Mar. 2017.

[8] A. Ahmedi, M. Barnes, V. Levi, J. C. Sanchez, C. Ng, and P. Mckeever, "Modelling of wind turbine operation for enhanced power electronics reliability," *IEEE Trans. Energy Convers.*, vol. 37, no. 3, pp. 1764–1776, Sep. 2022.

[9] A. A. Salem, N. A. N. Aldin, A. M. Azmy, and W. S. E. Abdellatif, "Implementation and validation of an adaptive fuzzy logic controller for MPPT of PMSG-based wind turbines," *IEEE Access*, vol. 9, pp. 165690–165707, 2021.

[10] S. Lim, D. Choi, S. H. Lee, C. Kang, and J.-W. Park, "Frequency stability enhancement of low-inertia large-scale power system based on grey wolf optimization," *IEEE Access*, vol. 10, pp. 11657–11668, 2022.

[11] H. T. Nguyen, G. Yang, A. H. Nielsen, and P. H. Jensen, "Combination of synchronous condenser and synthetic inertia for frequency stability enhancement in low inertia systems," *IEEE Trans. Sustain. Energy*, vol. 10, no. 3, pp. 997–1005, Jul. 2019.

[12] L. Badesa, F. Teng, and G. Strbac, "Conditions for regional frequency stability in power system scheduling—Part II: Application to unit commitment," *IEEE Trans. Power Syst.*, vol. 36, no. 6, pp. 5567–5577, Nov. 2021.

[13] L. Badesa, F. Teng, and G. Strbac, "Optimal portfolio of distinct frequency response services in low-inertia systems," *IEEE Trans. Power Syst.*, vol. 35, no. 6, pp. 4459–4469, Nov. 2020.

[14] W. Yan, L. Cheng, S. Yan, W. Gao, and D. W. Gao, "Enabling and evaluation of inertial control for PMSG-WTG using synchronverter with multiple virtual rotating masses in microgrid," *IEEE Trans. Sustain. Energy*, vol. 11, no. 2, pp. 1078–1088, Apr. 2020.

[15] J. Hu, L. Sun, X. Yuan, S. Wang, and Y. Chi, "Modeling of type 3 wind turbine with df/dt inertia control for system frequency response study," *IEEE Trans. Power Syst.*, vol. 32, no. 4, pp. 2799–2809, Jul. 2017.

[16] J. Ekanayake and N. Jenkins, "Comparison of the response of doubly fed and fixed-speed induction generator wind turbines to changes in network frequency," *IEEE Trans. Energy Convers.*, vol. 19, no. 4, pp. 800–802, Dec. 2004.

[17] M. Abdeen, M. Sayyed, J. L. Dominguez-Garcia, and S. Kamel, "Supplemental control for system frequency support of DFIG-based wind turbines," *IEEE Access*, vol. 10, pp. 69364–69372, 2022.
[18] N. R. Ullah, T. Thiringer, and D. Karlsson, "Temporary primary frequency control support by variable speed wind turbines—Potential and applications," *IEEE Trans. Power Syst.*, vol. 23, no. 2, pp. 601–612, May 2008.
[19] C. H. Lin and Y. K. Wu, "Overview of frequency-control technologies for a VSC-HVDC-integrated wind farm," *IEEE Access*, vol. 9, pp. 112893–112921, 2021.
[20] M. Kang, K. Kim, E. Muljadi, J. W. Park, and Y. C. Kang, "Frequency control support of a doubly-fed induction generator based on the torque limit," *IEEE Trans. Power Syst.*, vol. 31, no. 6, pp. 4575–4583, Nov. 2016.
[21] D. Yang, J. Kim, Y. C. Kang, E. Muljadi, N. Zhang, J. Hong, S.-H. Song, and T. Zheng, "Temporary frequency support of a DFIG for high wind power penetration," *IEEE Trans. Power Syst.*, vol. 33, no. 3, pp. 3428–3437, May 2018.
[22] Z. Lu, Y. Ye, and Y. Qiao, "An adaptive frequency regulation method with grid-friendly restoration for VSC-HVDC integrated offshore wind farms," *IEEE Trans. Power Syst.*, vol. 34, no. 5, pp. 3582–3593, Sep. 2019.
[23] M. Kheshti, L. Ding, W. Bao, M. Yin, Q. Wu, and V. Terzija, "Toward intelligent inertial frequency participation of wind farms for the grid frequency control," *IEEE Trans. Ind. Informat.*, vol. 16, no. 11, pp. 6772–6786, Nov. 2020.
[24] W. Bao, L. Ding, Z. Liu, G. Zhu, M. Kheshti, Q. Wu, and V. Terzija, "Analytically derived fixed termination time for stepwise inertial control of wind turbines—Part I: Analytical derivation," *Int. J. Electr. Power Energy Syst.*, vol. 121, Oct. 2020, Art. no. 106120.
[25] R. Yan, N.-A.-Masood, T. K. Saha, F. Bai, and H. Gu, "The anatomy of the 2016 South Australia blackout: A catastrophic event in a high renewable network," *IEEE Trans. Power Syst.*, vol. 33, no. 5, pp. 5374–5388, Sep. 2018.
[26] A. D. Hansen, F. Iov, P. Sørensen, N. Cutululis, C. Jauch, and F. Blaabjerg, "Dynamic wind turbine models in power system simulation tool," DIgSILENT, Gomaringen, Germany, Tech. Rep. Risø-R-1400(ed.2) (EN), 2007.
[27] B. Shen, B. Mwinyiwiwa, Y. Zhang, and B.-T. Ooi, "Sensorless maximum power point tracking of wind by DFIG using rotor position phase lock loop (PLL)," *IEEE Trans. Power Electron.*, vol. 24, no. 4, pp. 942–951, Apr. 2009.
[28] M. R. Aghamohammadi, S. F. Mahdavizadeh, and Z. Rafiee, "Controlled islanding based on the coherency of generators and minimum electrical distance," *IEEE Access*, vol. 9, pp. 146830–146840, 2021.
[29] J. Lee, E. Muljadi, P. Srensen, and Y. C. Kang, "Releasable kinetic energy-based inertial control of a DFIG wind power plant," *IEEE Trans. Sustain. Energy*, vol. 7, no. 1, pp. 279–288, Jan. 2016.

SUNGHOON LIM (Member, IEEE) received the B.S. and Ph.D. degrees from the Department of Electrical Engineering, Yonsei University, Seoul, South Korea, in 2018 and 2022, respectively. He is currently a Postdoctoral Research Associate with the School of Electrical and Electronic Engineering, Yonsei University. His current research interests include wind-turbine generator system control, power system stability, and optimization.

DONGHEE CHOI (Member, IEEE) received the B.S. and Ph.D. degrees in electrical engineering from the School of Electrical and Electronic Engineering, Yonsei University, Seoul, South Korea, in 2012 and 2017, respectively. From 2017 to 2018, he was a Postdoctoral Research Associate with the School of Electrical and Electronic Engineering, Yonsei University. He was one of few who had been selected for a Postdoctoral Training (Fostering Next-generation Researcher Program, in 2017) at the National Research Foundation (NRF), South Korea. He was also a Manager with the Energy Storage System (ESS) Team, Smart Energy Unit, Future Convergence Business Office, Korea Telecom (KT), Seoul. He is currently an Assistant Professor of electrical and control engineering with the Division of Converged Electronic Engineering, Cheongju University, Cheongju-si, South Korea. His research interests include power system dynamics, power system stability, and operation and control and stand-alone microgrid operation.

JUNG-WOOK PARK (Senior Member, IEEE) was born in Seoul, South Korea. He received the B.S. degree *(summa cum laude)* from the Department of Electrical Engineering, Yonsei University, Seoul, in 1999, and the M.S.E.C.E. and Ph.D. degrees from the School of Electrical and Computer Engineering, Georgia Institute of Technology, Atlanta, GA, USA, in 2000 and 2003, respectively. From 2003 to 2004, he was a Postdoctoral Research Associate with the Department of Electrical and Computer Engineering, University of Wisconsin–Madison, Madison, WI, USA. Since 2005, he has been with the School of Electrical and Electronic Engineering, Yonsei University, where he is currently a Professor. He is also the Director at the Yonsei-Power System Research Center of Great Energy Transition (Yonsei-PREFER) supported by the leading research program (with the $7.2M USD grant for nine years, from 2020 to 2029) of the National Research Foundation (NRL), South Korea. His current research interests include power system dynamics, energy management systems, renewable energies-based distributed generation systems, operation and planning of microgrid, and hardware implementation of power-electronic based inverters. He was a recipient of the Young Scientist Presidential Award from the Korean Academy of Science and Technology (KAST), South Korea, in 2013.